THE COULOMB POTENTIAL OR SCATTERING CHAOS IN A NON-GÈNERIC CASE*

L. WIESENFELD**

LAGRIPPA† DRF-MC, Centre d'Etudes Nucléaires de Grenoble
85X, 38041 Grenoble, France

(Received January 29, 1992)

Among the various systems that are analyzed in terms of Hamiltonian chaos, the Coulomb potential perturbed by an external electro-magnetic field is of special importance in microscopic physics. We present here a view of the group-theoretical techniques that have been used in order to reduce the non-integrable dynamics to its smallest possible extent. Chaotic diffusion in a driven Coulomb potential is analyzed and results presented: fixed points, periodic orbits, deflection functions, inelastic cross-sections. The essentially mixed character of phase space is underlined. As a foreseeable consequence, the deflection function *does not* display a full self-similar structure after a few generations in the fractal structure.

PACS numbers: 05.45.+b, 03.65.Fd, 03.65.Nk

1. Introduction

On several instances in this conference has the topic of *chaotic scattering* been addresed to, in different contexts. From the general classical and semi-classical considerations of Jung, a precise definition of the chaotic saddle (chaotic repellor) may be drawn, that explains the fractal array of singularities in deflection functions and classical cross-sections. Global characterization of Hamiltonian chaos is especially easy in the case of chaotic

* Presented at the IV Symposium on Statistical Physics, Zakopane, Poland, September 19–29, 1991.

** New and permanent address : Laboratoire de Spectrométrie Physique, Université Joseph-Fourier, B.P.87, F-38402 St-Martin-d'Hères, France.

† A joint CNRS/CEA laboratory.

diffusion, as almost all trajectories spend only a finite period of time within the system. The outgoing asymptotic motion acts as a projection tool of the finite distance properties towards the plane at infinity, which coincides with the observation region. As was explained by Tèl and Stoop, this finite observation window allows one to extract useful global information about the classical chaos directly connected with the asymptotic regions, through the knowledge of deflection functions and cross-sections. It is most probable that in quantum mechanics, too, the information about quantum chaos — whatever this exactly means — should be readily extracted from asymptotic properties as opposed to bound eigenstates (see [1]).

We shall here emphasize different aspect of scattering chaos. We shall try to implement several of the general, successful ideas of hyperbolic scattering chaos into an essentially non-hyperbolic system, the perturbed Coulomb system.

The pure Coulomb system, with its long range $1/r$ potential, is at the cornerstone of the microscopic understanding of chaos, theoretically and experimentally. Very detailed work has been achieved in both the diamagnetic and driven atomic hydrogen systems, which test several aspects of the classical, semi-classical and quantum approaches to highly symmetric, strongly perturbed systems. In the diamagnetic case which, in the author's opinion, is well understood, it is through a full analysis of the dynamical symmetry of the Coulomb system that progress could be made, both conceptually and technically. In the driven case, full understanding is not at hand, despite the very large amount of work. As due to the infinity of bound trajectories that are supported by this non-linear oscillator, that extent from 0 to ∞, every external frequency is in resonance only with a fraction of the bound system, leaving tightly *and* loosely bound states untouched. Phase space is of intrinsic mixed character, with all its hierarchy of stable islands and islets. On the other hand, the high symmetry of the problem at hand allows one to construct representation that incorporate a lot of information about invariant quantities, and that are tailored for the perturbation to be as constrained as possible.

We divide that report into two sections. Section 2 tries to give the reader a glimpse on the different dynamical symmetries of the Coulomb system, and to begin with, its 4D harmonic oscillator image. Introduction of the perturbation in different representation is described. In Section 3, our own results in the scattering chaos will be presented, along with the derivation of a divergence- and ambiguity-free representation. Some provisional conclusions end this report.

2. Symmetries of the Coulomb system

2.1. Dynamical group

Let us start with the usual Coulomb Hamiltonian, adopting the same framework for quantum or classical mechanics:

$$\mathcal{H} = \frac{\boldsymbol{p}^2}{2m} - \frac{1}{4\pi\epsilon_0}\,\frac{Ze^2}{r}. \tag{1}$$

We implicitely assume that the two-body motion of two charged particles moving under mutual influence and subjected to an external field may be reduced to the motion of a test particle, mass m, in a pure Coulomb potential, and some external influence. A discussion of that reduction will be put forward in the next Chapter. Our first task is to find the most complete and systematic way to take into account all the symmetries hidden in this innocent-looking Hamiltonian. In doing so, any perturbation of that Hamiltonian should be recast into the symmetry elements of the Coulomb problem. Also, this approach should give us at the end clues about adiabatically conserved quantities, if any. The procedure rests mainly in an algebraic recasting of the Hamiltonian in Lie group generators; this group should describe as accurately as possible all the symmetries present in the problem, when described in phase space. The material presented here has been known for some of its aspects for a fairly long time. The 4D symmetry of atomic hydrogen dates back to Pauli [2] and Bragmann [3]; dynamical group properties, which connect trajectories wavefunctions or matrix elements at different energies, have also been known by physicists since the sixties, [4], particularly by the works of Barut [5]. A recent and particularly lucid presentation of the atomic hydrogen symmetry may be found (in French !) in Ref. [6], on which this Section rests heavily. We shall thus develop here a particular representation of some of the Coulomb Hamiltonian symmetries. That representation is well adapted to the different problems at hand, and makes explicit the connection between the Coulomb and the harmonic oscillators. The reader interested in more general derivations should consult the references cited above.

Let us first get rid of the physical constants, by switching to atomic units:

$$\hbar = |e| = m = 4\pi\epsilon_0 = 1,$$

$$c = 1/\alpha \simeq 137.$$

Unit of length is of course Bohr's radius $a_0 = 0.529$ Å; unit of electric field is $F_0 = 5.14\ 10^9$ V/cm. With $Z = 1$, the Hamiltonian (1) reads:

$$\mathcal{H} = \frac{\boldsymbol{p}^2}{2} - \frac{1}{r}. \tag{2}$$

The traditionnal way of deriving the properties of $\mathcal{H}$ is to write it down in some system of coordinates, say spherical, and — clasically — to find the corresponding actions. Equivalently, one separates the Hamilton-Jacobi equations. This is the normal access towards a semi-classical quantization, following the Einstein–Brillouin–Kramers scheme [7]. One has, in spherical coordinates r, θ, ϕ :

$$\mathcal{H} = \frac{1}{2}\left(p_r^2 + \frac{p_\theta^2}{r^2} + \frac{p_\phi^2}{r^2 \sin^2\theta}\right) - \frac{1}{r}. \tag{3}$$

To each coordinate corresponds an action, noted I_r, I_θ, I_ϕ. Upon substitution by their expression in terms of r, θ, ϕ, one gets the following Hamiltonian (for negative energies, *i.e.* bound motion):

$$\mathcal{H} = -2\pi^2 \left(I_r + I_\theta + I_\phi\right)^{-2}. \tag{4}$$

Quantization of these actions leads to the usual quantum numbers n_r, ℓ, m. That the full symmetry has not been taken into account is obvious, as the three characteristic frequencies in this representation are degenerate : $\omega = \omega_i, \forall i$, where $\omega_i = -\partial\mathcal{H}/\partial I_i$, $i = r, \theta, \phi$. This is the exact classical analog of the so-called "accidental" degeneracy in n^2 for the atomic hydrogen levels. This degeneracy is fully explained if we recall that both the angular momentum $\boldsymbol{L} = \boldsymbol{r} \times \boldsymbol{p}$ and the Runge–Lenz vector $\boldsymbol{A} = \boldsymbol{p} \times \boldsymbol{L} - \boldsymbol{r}/r$ are conserved quantities. Let us define $\boldsymbol{A}' = \boldsymbol{A}/\sqrt{|2E|}$. One has the following algebra, where [,] denotes a Poisson bracket, classically, or a commutator, quantum mechanically ($i, j = 1, 2, 3$; ϵ_{ijk} is the fully antisymmetic tensor):

$$\begin{aligned} [L_i, L_j] &= i\epsilon_{ijk}\, L_k, \\ [L_i, A'_j] &= i\epsilon_{ijk}\, A'_k, \\ [A'_i, A'_j] &= \pm i\epsilon_{ijk}\, L_k. \end{aligned} \tag{5}$$

Sign + is for negative energies and sign − for positive ones. These structures are the ones that define so(4) ($E > 0$) or so(3,1) ($E < 0$)) Lie algebras, leading to a SO(4) (resp. SO(3,1)) symmetry of the bound (resp. unbound) Coulomb problem. It explains the complete degeneracy of the levels, which are fully characterized by one sole quantum member n, or equivalently, by one action I, in terms of which all observables that do not lift the degeneracy may be recast.

Now let us follow a heuristic approach in order to make clear the analogy between the Coulomb oscillator and the coupled harmonic oscillator problems. In order to simplify the representation, we particularize one axis, say O_z, and just consider invariance around that direction. It means that

we consider the following subgroup chain: $SO(4) \supset SO(3)_L \supset SO(2)_{L_z}$. Let us begin in the natural cylindrical coordinates ($r^2 = \rho^2 + z^2; L_z = m_z$):

$$\mathcal{H} = \frac{p_\rho^2}{2} + \frac{p_z^2}{2} + \frac{m_z^2}{\rho^2} - \frac{1}{r}. \tag{6}$$

We introduce now semi-parabolic coordinates in order to regularize the Coulomb motion nearby the origin:

$$\mu^2 = r + z; \quad \nu^2 = r - z. \tag{7}$$

We get:

$$\mathcal{H} = \frac{1}{2(\mu^2 + \nu^2)} \left(p_\mu^2 + \frac{m_z^2}{\mu^2} - 2 + p_\nu^2 + \frac{m_z^2}{\nu^2} - 2 \right). \tag{8}$$

Motions in μ and ν decouple if we introduce the new generator $\widetilde{\mathcal{H}}$, and extend phase space:

$$\begin{aligned} 0 \equiv \widetilde{\mathcal{H}} &= (\mathcal{H} - E)(\mu^2 + \nu^2) \\ &= \frac{1}{2} \left(p_\mu^2 + \frac{m_z^2}{\mu^2} - 2E\mu^2 \right) + \frac{1}{2} \left(p_\nu^2 + \frac{m_z^2}{\nu^2} - 2E\nu^2 \right). \end{aligned} \tag{9}$$

This amounts to a change of time t as an independent variable to a fictitious time τ, with:

$$\frac{d\tau}{dt} = \frac{1}{\mu^2 + \nu^2}. \tag{10}$$

Consequently, we have, in time τ, *two rotating 2D harmonic oscillators*, with an identical frequency $\Omega = (-2E)^{1/2}$. For $E > 0$, it leads to repulsive harmonic oscillators, whose solutions are the hyperbolic lines. One has (for $L_z = 0$, for simplicity):

bound motion	unbound motion
$\mu = (-2E)^{-1/2} \cos \Omega\tau/2$	$\mu = (2E)^{-1/2} \cosh \Omega\tau/2$
$p_\mu = 2 \sin \Omega\tau/2$	$p_\mu = 2 \sinh \Omega\tau/2$
$\nu = (-2E)^{-1/2} \cos(\Omega\tau/2 + \Delta\phi)$	$\nu = (2E)^{-1/2} \cosh(\Omega\tau/2 + \delta\phi)$
$p_\nu = 2 \sin(\Omega\tau/2 + \Delta\phi)$	$p_\nu = 2 \sinh(\Omega\tau/2 + \Delta\phi)$

One sees that, when comparing these equations with the solutions of the Coulomb equation in ordinary space, recalling the relations (7) — e is the eccentry:

bound motion	unbound motion
$r = (-2E)^{-1}(1 - e\cos u)$	$r = (2E)^{-1}(1 - e\cosh u)$
$p^2 = (-2E)\dfrac{\sin^2 u + (1-e^2)\cos^2 u}{(1-e\cos u)^2}$	$p^2 = (2E)\dfrac{-\sinh^2 u + (1-e^2)\cosh^2 u}{(1-e\cosh u)^2}$
$t = T(u - e\sin u)$	$t = T(e\sinh u - u)$

the ficticious time τ is in fact proportional to the anomalic eccentry $u = \Omega\tau/2$. In this representation, the total symmetry of the original system is $O(3) \supset O(2) \otimes O(2)$, that is the restriction of the full O(4) symmetry by the $L_z = \text{cte}$ condition. Moreover, it is easier in this picture to find out the dynamical group associated with those two harmonic oscillators: now we still keep O_z as a particular invariant direction in space, but let the energy vary. The dynamical group associated with one 2D oscillators is SO(2,1)[1]. One of the generator (namely $S_2^{(\alpha)}$) is a dilatation operation which directly connects levels of different energies. The two oscillators coupled together yield the total dynamical symmetry $SO(2,2) = SO(2,1)_\mu \otimes SO(2,1)_\nu$. All trajectories (or levels, matrix elements) are connected together by successive operation of the group generator, as long as they share the same L_z (or m_z).

2.2. Perturbation

The preceeding Section has shown how peculiar the Coulomb system is, with respect to group properties. Its symmetry is so large (SO(4,2)) that an external field does not suppress it altogether. As a consequence, the phase space remains of mixed character, with regular motion dominating parts of it. Even for a very strongly perturbed H atom, the doubly excited He**, is the symmetry not fully broken, and large islands of regular motion persist [9].

2.2.1. Diamagnetic Coulomb problem

The image of the two oscillators, running at a same frequency and

---

[1] Generators for $L_z = 0$ are (α, a parameter):

$$\begin{cases} S_1^{(\alpha)} = -\frac{\alpha}{4}p_\mu^2 + \frac{1}{4\alpha}\mu^2 \\ S_2^{(\alpha)} = -\frac{1}{2}\mu p_\mu \\ S_3^{(\alpha)} = +\frac{\alpha}{4}p_\mu^2 + \frac{1}{4\alpha}\mu^2 \end{cases} \qquad \begin{cases} \left[S_1^{(\alpha)}, S_2^{(\alpha)}\right] = +S_3^{(\alpha)} \\ \left[S_2^{(\alpha)}, S_3^{(\alpha)}\right] = -S_1^{(\alpha)} \\ \left[S_3^{(\alpha)}, S_1^{(\alpha)}\right] = -S_2^{(\alpha)} \end{cases}$$

Casimir operator: $S_3^2 - S_2^2 - S_1^2 = 0$. Lie algebra: so(2,1).

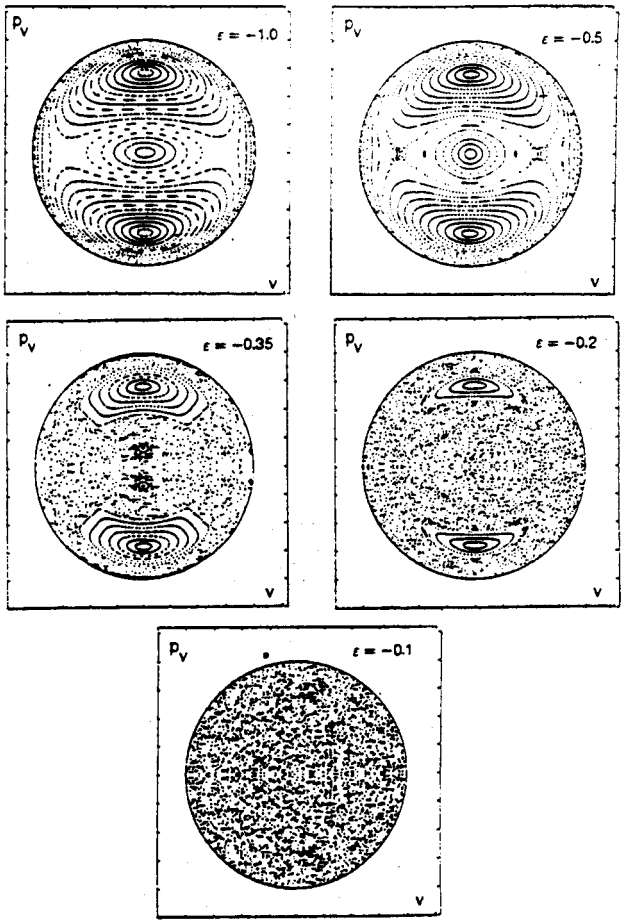

Fig. 1. Poincaré sections in the μ, p_μ plane (here labelled as v, p_v), showing the progressive disappearence of elliptic islands with increasing γ (from Ref. [10]).

keeping the same relative phase is very useful to show how perturbations will destroy that nice integrable motion. The diamagnetic Coulomb problem has been considered for a long time as a paradigmatic example for chaos in the microscopic world (see [8,10] for recent reviews). In atomic units, with γ the reduced magnetic field, the Hamiltonian reads:

$$\tilde{\mathcal{H}} = \tilde{\mathcal{H}}_{\rm osc}(\mu) + \tilde{\mathcal{H}}_{\rm osc}(\nu) + \frac{1}{8}\gamma^2\mu^2\nu^2(\nu^2+\mu^2), \tag{11}$$

where $(\chi = \mu, \nu)$

$$\tilde{\mathcal{H}}_{\rm osc}(\chi) = \frac{p_\chi^2}{2} + \frac{m^2}{\chi^2} - 2E\chi^2. \tag{12}$$

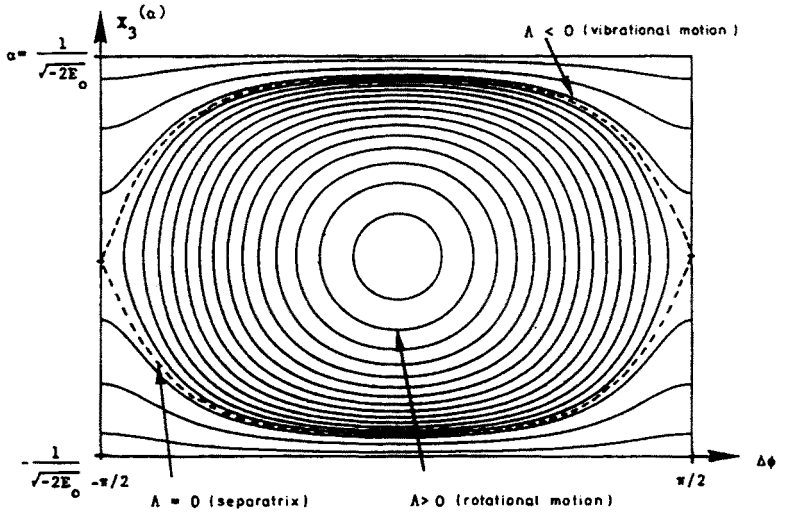

Fig. 2. Poincaré sections in the μ, p_μ plane, showing the regularity of the orbits, when the Λ quantity is an adiabatic invariant (from Ref. [6]). $X_3^{(\alpha)} = S_3^{(\alpha)} - T_3^{(\alpha)}$, difference in energy of the two oscillators; $\Delta\phi$ is its associated phase.

The coupling comes about with two sextic terms in μ, ν. A full series of Poincaré sections, showing the progressive disappearance of elliptic islands have been published (in [10], for example) (see Fig. 1). Large quantum calculations are made possible in the framework of Lie group generators representations. From the knowledge of the full dynamical symmetry, matrix elements are constructed that bind all relevant states, by successive applications of the Wigner–Eckhardt theorem. Also continuum and bound state wavefunctions are built in the same discrete basis of Sturmian functions, and related to each other by dilatation operator belonging to the full

dynamical symmetry (for example $S_2^{(\alpha)}$). Results and comparison with experiments on lithium are to be found in [11,12]. More interestingly, by use of the proper generators of SO(2,2) dynamical symmetry, Delande obtained readily the adiabatic invariants of the motion, by calculating the mean value of $\Lambda = \langle \mu^2 \nu^2 (\mu^2 + \nu^2) \rangle$ over one cycle of the angular variables associated with SO(2,2). An example of phase space is shown in Fig. 2.

2.2.2. Driven Coulomb problem

We couple now the two oscillators with a time dependent perturbation. Recalling that the μ and the ν oscillators vibrate at the same frequency $\Omega = \sqrt{-2E}$, the coupling comes about as $-E$ is the conjugate variable to t; that isosynchronism is here the driving mechanism. In the non-relativistic appproximation [13], with a linearly polarized electric field $F \cos \omega t$, the Hamiltonian reads:

$$\tilde{\mathcal{H}} = \tilde{\mathcal{H}}_{\text{osc}}(\mu) + \tilde{\mathcal{H}}_{\text{osc}}(\nu) + \frac{F}{2} \left(\mu^4 - \nu^4\right) \cos \omega t. \tag{13}$$

This Hamiltonian, often recast in usual coordinates, serves as a basis for the numerous calculations pertaining to the ionisation of excited hydrogen by microwaves (see next paragraph). However, there has not been, to the best of the author's knowledge, any systematic attempt to rewrite a classical/quantum calculation into group-symmetry adapted coordinates or even into the double pendulum picture. It is clear that only such an approach, besides its built-in regularization, would yield the right adiabatic invariants at once, if any exists. A fully algebraic approach is thus lacking[2].

We shall thus in this report resort either to ordinary or to regularized coordination in order to represent the motion, and to action-angle variables to analyze it. However, as stated above, no attempt has been made to formulate the driven Coulomb motion fully into the invariance or dynamical group generators.

3. The driven Coulomb problem: Scattering chaos

3.1. Introduction

Considerable amounts of work have been devoted to study and understand the dynamics of excited hydrogen in an intense micro-wave field:

$$\mathrm{H}^* + N\, h\nu \longrightarrow \mathrm{H}^+ + \mathrm{e}^- + M\, h\nu.$$

[2] Let us note in passing that large amounts of work have been devoted to group theoretical techniques and chaos in vibrating molecules [17,18].

Many experiments, classical and quantum calculations have been performed, in the slow or fast driving frequencies regimes ($\omega_{\text{driving}} \lesssim \Omega_{\text{Kepler}}$). We shall not attempt here to summarize the numerous results; for reviews, see [21,22]. Many important results have been obtained; the validity of classical/semi-classical approximations has been precised. Quantum localisation appeared as a relevant concept.

Here, we shall deal only with the scattering part of the classical phase spaces, that is, we shall deliberately ignore both the quantum effects and the tightly bound orbits. Experimentally, hints of chaotic scattering have very recently appeared in the litterature, in plasma physics [19] or in cooled ions experiments [20].

3.2. Scattering chaos - generalities

Let us recall the assumptions we make in order to analyse the inelastic scattering process:

$$e^-(E) + H^+ \xrightarrow{\text{e.m.field}} e^-(E') + H^+.$$

We suppose that [13,14]:

a. the oscillatory electro-magnetic field is classical, linearly polarized along the incoming electron motion (O_z);
b. the ions are sufficiently far apart so that screening of the Coulomb potential is unphysical[3];
c. the oscillatory field does not die out at infinity, so that no spurious non-linearity is introduced, through ponderomotive potential gradients;
d. oscillatory field intensity is low enough to neglect all relativistic effects: B fields, self-forces;
e. the mass of the ion is infinite; no recoil is taken into account.

In this framework, the Hamiltonian reads, in length-gauge (atomic units):

$$\mathcal{H} = \frac{p^2}{2} - \frac{1}{r} + Fz\cos\omega t. \tag{14}$$

These assumptions (b–e) are the ones under which all calculations have undertaken up to now. Also a reduction to discrete maps (the so-called Kepler Map) is particularly useful in 2D and in 1D configurational spaces, for exploring the quantum regimes [22]. Here we shall deal only with the

[3] This is the situation prevailing in low-density ionic beams, such as those emerging form Electron-Cyclotron-Resonance sources.

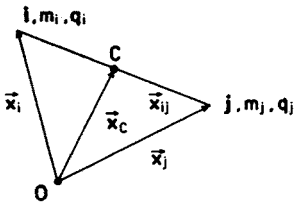

Fig. 3. Center-of-mass and relative coordinates

scattering part of the classical phase space, that is, we shall ignore both quantum effects and thightly bound orbits.

It is quite instructive to precise now the exact realm of the potential approach to this driven two-body problem. Let us first suppose that the two particles i and j have equal masses (Fig. 3). Center of mass is $\boldsymbol{x}_C = (\boldsymbol{x}_i + \boldsymbol{x}_j)/2$; relative coordinate $\boldsymbol{x}_{ij} = (\boldsymbol{x}_i - \boldsymbol{x}_j)$. We have the following Newton equations, with q_i, q_j the charges and $Q = q_i q_j$ (in atomic units):

$$\begin{cases} \ddot{\boldsymbol{x}}_i = Q \dfrac{\boldsymbol{x}_{ij}}{|\boldsymbol{x}_{ij}|^3} + q_i \boldsymbol{F} \cos \omega t, \\ \ddot{\boldsymbol{x}}_j = Q \dfrac{\boldsymbol{x}_{ji}}{|\boldsymbol{x}_{ij}|^3} + q_j \boldsymbol{F} \cos \omega t, \end{cases} \tag{15}$$

yielding :

$$\begin{cases} \ddot{\boldsymbol{x}}_C = 0 + \frac{1}{2}(q_i + q_j)\, \boldsymbol{F} \cos \omega t, \\ \ddot{\boldsymbol{x}}_{ij} = 2Q \dfrac{\boldsymbol{x}_{ij}}{|\boldsymbol{x}_{ij}|^3} + (q_i - q_j)\, \boldsymbol{F} \cos \omega t. \end{cases} \tag{16}$$

We note that for $m_i = m_j$ and $q_i = q_j$, motion is separable, at least in this non-relativistic limit. This is the all-important case of electron-electron and proton-proton scattering, in the presence of a moderately intense laser field[4]. Also, if $m_i \neq m_j$, but $q_i = q_j$, the relative motion remains integrable, *i.e.* $e^+ - H^+$ scattering (a physical reason for this absence of chaos is the absence of bound Coulomb states). However, as soon as $q_i \neq q_j$ either the c.o.m. or the relative notion become chaotic. In order to restrict the number of physical parameters, let us recall now the classical scaling laws,

[4] For example, dynamics of the electrons in the free electron laser is integrable is the absence of $\boldsymbol{B}$ field, as long as the kinematics remain non relativistic. The author knows no exemple of chaos analysis in the relativistic domain.

which pertain to Kepler motion and harmonic driving [14,15]. Dynamics remains unchanged when scales are modified according to:

$$\begin{cases} r \to \gamma r \\ t \to \gamma^{3/2} t \\ p \to \gamma^{-1/2} p \\ \mathcal{H} \to \gamma^{1} \mathcal{H} \end{cases} \qquad \begin{cases} F \to \gamma^{-2} F \\ \omega \to \gamma^{-3/2} \omega \\ \mathcal{P} \to \gamma^{4} \mathcal{P} \end{cases} \tag{17}$$

where $\mathcal{P}$ in the laser power (or energy flux). As a consequence, structure of phase space is determined by one scale-invariant parameter, say $F\omega^{-4/3}$, and one trajectory is fixed by another independent scale-independent condition, as $I\omega^{-3}$ [23]. I, the action, scales as $I \to \gamma^{1/2} I$, so that scaling properties *do not* translate into quantum mechanics, which sets an absolute scale through $\hbar$.

Before embarking on real calculations, some short comments are in order to discuss dimensionality. For linear polarization of the $\boldsymbol{F}$ field, parallel to incoming electron momentum $\boldsymbol{p}$, the classical problem is clearly 2D in configuration space, yielding 6D extended phase space. Consequently, the 4D Poincaré or plane at infinity sections are too complicated do depict. However, some qualitative work has shown that a chaotic saddle exists in the 6D phase space [13]. We restrict ourselves in the following to 1D configurationnal space (back-scattering, $\ell = 0$ quantum state), yielding 4D extended phase space and 2D sections. In the two oscillators pictures, we retain only one of them, namely μ. The physical quantity of interest, inelastic cross-sections are of the form (Ω, solid angle):

$$\frac{d^2\sigma}{d\Omega\, dE} \to \frac{d\sigma}{dE}\ (\Omega = 0). \tag{18}$$

The discussion that follows is divided into the following sections: Section 3.3. is devoted to the finite distance properties of the driven Coulomb potential, derived in regularized coordinates and depicted in stroboscopic Poincaré sections. Section 3.4. explains briefly the techniques needed to get rid of unnecessary infinities and oscillations when studying asymptotic properties; these are presented in Section 3.5. (deflection functions, cross-sections). Some comparison with elementary quantum-mechanical treatment are presented by then.

3.3. Finite distance properties

As mentioned in the previous Section, one scale-independent parameter determines the overall dynamics at hand (structure of the Poincaré section). An analysis of the main resonances appeared some time ago [23]. We shall present here an overview of results obtained at a sufficiently weak field

($F\omega^{-4/3} \simeq 0.1$) so that both stable and unstable periodic orbits survive at finite distance. In order to represent trajectories hitting the $r \to 0$ singularity, one has to resort to regularized coordinates equivalent to the oscillator picture (retaining μ, Eq. (9)); the Hamilton equations read:

$$\begin{cases} \dot{\mu} = p_\mu, \\ \dot{p}_\mu = 2E\mu - 2F\mu^3 \cos\omega t, \\ \dot{t} = \mu^2, \\ \dot{E} = -\frac{1}{2} F\omega\mu^4 \sin\omega t, \end{cases} \tag{19}$$

where t and E are considered as dynamical quantities and the dot denotes $d/d\tau$. For $F = 0$, phase space looks like Fig. 4.

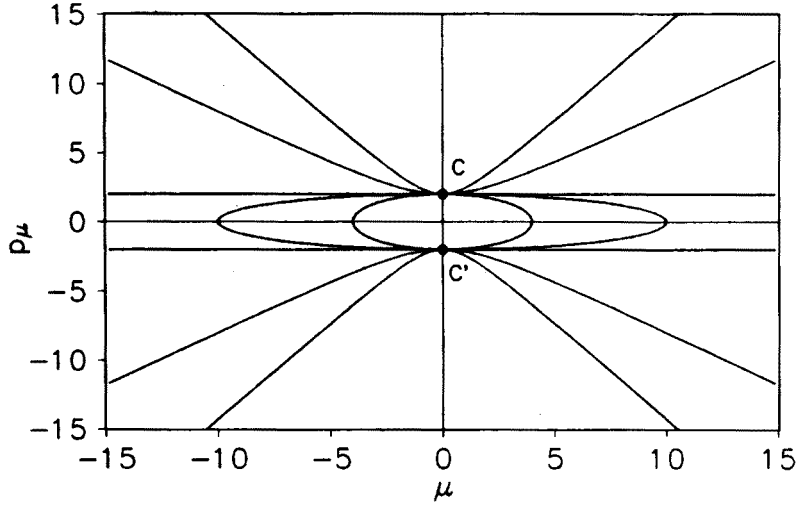

Fig. 4. Phase space of the Coulomb oscillator in the μ, p_μ representation, in the absence of F field. Points C, C', coordinates $\mu = 0$, $p_\mu = \pm 2$ are both representing the origin. In ordinary phase space, it corresponds to $r = 0$, $p_r \to \pm\infty$. The ellipses are the bound trajectories, the two straight lines, the zero-energy trajectory and the hyperbolas, the scattering ones.

The origin is a symmetry center: (μ, p_μ) is identical to $(-\mu, -p_\mu)$. One recognizes in Fig. 5 the bound, unbound and zero energy trajectories in an attractive Coulomb potential. Fig. 5 shows full trajectories in μ, p_μ plane and Figs 6, 7 a full trajectory in the r, t plane. All the peculiarities of the harmonically driven Coulomb potential show up here: coexistence of thightly and loosely bound trajectories, with vastly different resonance frequencies; exchange of energy occuring only nearly the origin; asymptotic motion that is a simple superposition of Coulomb drift + oscillatory motion. The chaotic saddle lies thus in between the tightly bound trajectories,

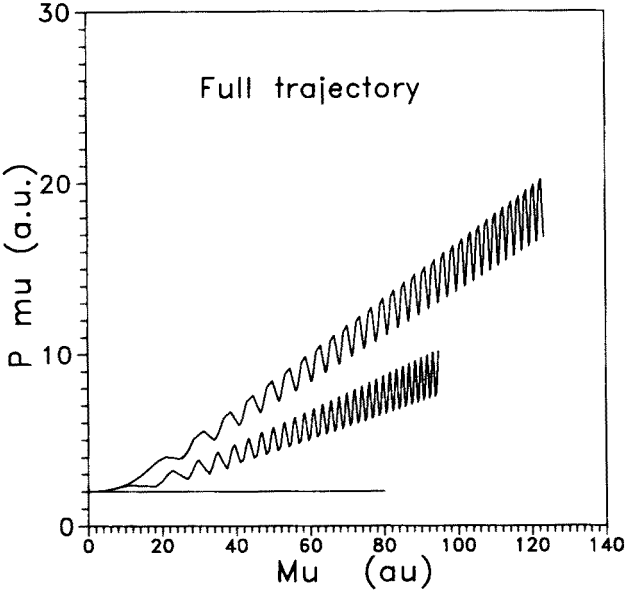

Fig. 5. A trajectory in μ, p_μ phase space, in the presence of Coulomb and driving field.

nearly unperturbed for these relatively weak fields and the loosely bound trajectories, that bear no non-linear coupling between fields.

Fig. 8 support these views: it shows two stroboscopic Poincaré sections in the μ, p_μ plane, at $\omega t = \pi/2$. Each trajectory has an identical energy at infinity, bu they differ in their phase with respect to the driving field (see next Section for a precise definition of those quantities). The one trajectory shown with crosses ($\times$) is immedialtely sent away after one reflection, with a slightly higher energy, while the other trajectory, shown with triangles ($\triangle$) undergoes several reflections and goes through some three Rydberg states before being sent off with a slightly lower energy.

A Poincaré section of innermost part of the phase space is shown in Fig. 9. It differs from analogous figures from the works of Richards [23] by the choice of the stroboscopic phase: we chose $\omega t = \pi/2$ *vs* $\omega t = 0$; see also Jensen *et al.* [21] who presented an analogous figure, but in the r, p plane, where the singularity at $r \to 0, p \to \infty$ makes interpretation less easy. Also shown in Fig. 9 are the first periodic orbits, stable and unstable, of periods 1 and 2 (recall the symmetry $\mu, p_\mu \leftrightarrow -\mu, -p_\mu$). Some orbits are shown in Figs 10–11, through a Lissajous plot $\mu(t) = \mathcal{L}(F \cos \omega t)$. The stable or unstable character of a given orbit is readily apparent; the force exerted on the particle are on the one hand, the driving force $-F \cos \omega t$, and on the other hand, the restoring force $-1/\mu^4$. The restoring force and the driving force add up to pull back the particle towards the origin in the

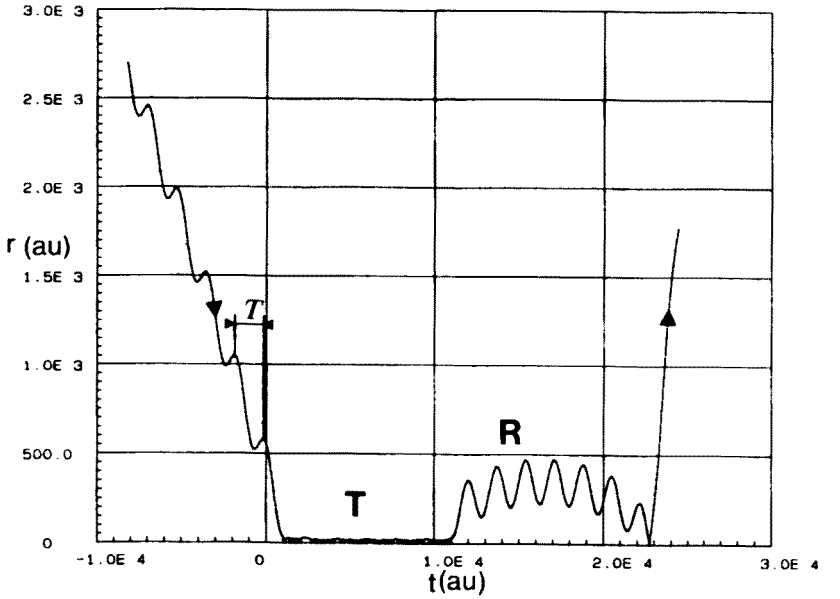

Fig. 6. A trajectory in configurational space $r = r(t)$. It displays all peculiarities of the Coulomb scattering: 1. far from the origin, a simple linear superposition of oscillations, amplitude quivering length $l = F/\omega^2$; 2. exchange of energy only nearby the origin; 3. two kinds of bound states, either tightly bound, weakly influenced by the driving field $\langle r \rangle \simeq 10 \ldots 15$a.u., or loosely bound (Rydberg state) and intermediate influence of both fields. T is the period of the driving field; **T** and **R** are the classical analogues of respectively a tightly bound or a Rydberg state. A detail is found in Fig. 7.

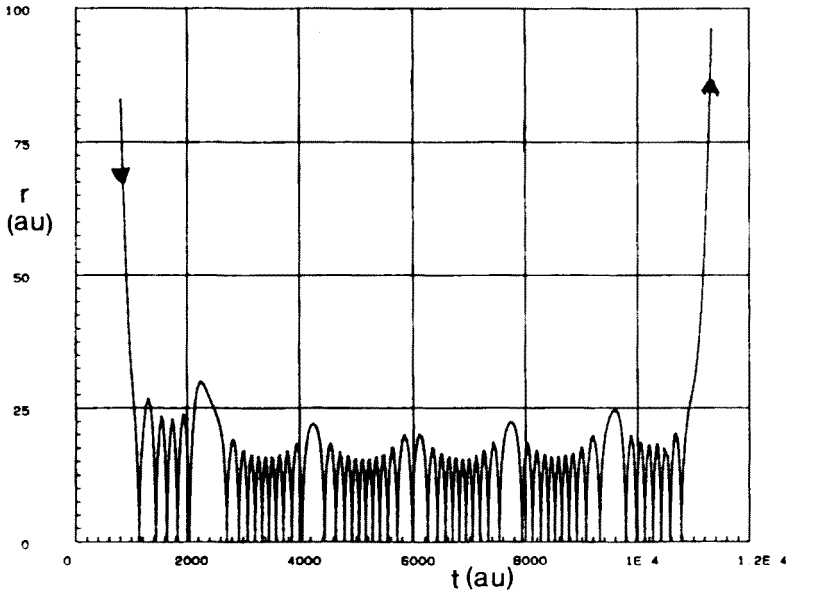

Fig. 7. Detail of Fig. 6, showing the tight part of the trajectory.

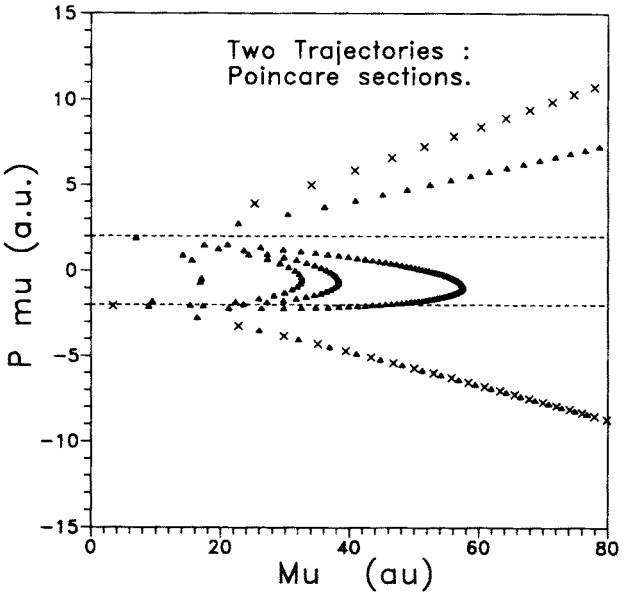

Fig. 8. Two stroboscopic Poincaré sections. Both trajectories have the same asymptotic energy, but differ in their phase ψ (Eq. (29)).

stable orbit of period 1, or for most part of the stable orbit of period 2. On the contrary, just a delicate balance of them both makes the unstable orbits periodic, as driving and restoring forces act one against the other, Fig. 10. Also the beginning of a symbolic dynamics appears here, as to a period 1–2 corresponds 1–2 oscillations in this Lissajous picture.

3.4. Symmetry-adapted Hamiltonian

On the Hamiltonian (14), several transformations have to be performed in order to get finite quantities in the asymptotic plane, defined independently of the driving field phase. We shall present here only a brief sketch of the sequence of canonical transformations, leaving to reference [16] the details.

First, let us get rid of the explicit time dependence of the Hamiltonian, by the usual extension of the phase space: $\{r, p_r\} \mapsto \{r, p_r; t, -E\}$. The new motion generator $\tilde{\mathcal{H}} = \mathcal{H} - E$ is a constant of motion, set arbitrarily to zero. Consequently $-E$ is just the energy of the driving field. We label that energy by $N = E/\omega$, the action of the field; time is then labelled by $\phi = \omega t$, the associated angle of the field. In velocity gauge, we get (atomic units):

$$0 \equiv \tilde{\mathcal{H}}_{\mathrm{V}} = \frac{1}{2}\left(p_{\mathrm{V}} + \alpha A \sin\phi\right)^2 - \frac{1}{r_{\mathrm{V}}} + N_{\mathrm{V}}\omega, \tag{20}$$

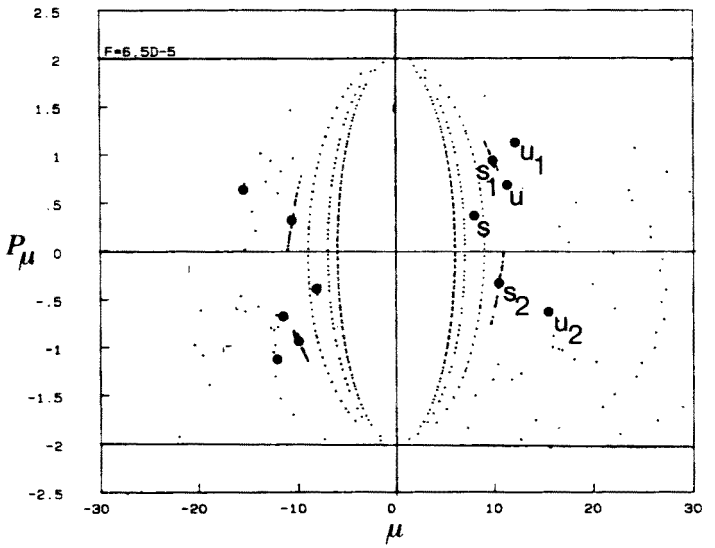

Fig. 9. *Inner Poincaré section.* Phase reference: $\phi = \pi/2$. Parameters in atomic units: $F = 6.5\,10^{-5}$, $\omega = 0.004$. Shown are the first periodic orbits: **S**, stable, period 1; **U**, unstable, direct hyperbolic, period 1; **S1, S2**, stable, period 2; **U1,U2**, unstable, inverse hyperbolic, period 2. The last full KAM torus encircles **S** but leaves **S1, S2** outside.

p_V, r_V have their usual meaning in velocity gauge; A is the vector potential. In order to get rid of the linear superposition of oscillatory motion and Coulomb drift, in the asymptotic domain, it is quite usual to opt for another gauge, the acceleration gauge [33], defined as:

$$\begin{cases} r_A = \rho - l\cos\phi = r_V - l\cos\phi, \\ p_A = \pi + l\omega\sin\phi = p_V, \end{cases} \tag{21}$$

ρ, π are the ordinary position and velocity. $l = F/\omega^2$ is the quivering length. Absorbing the instantaneous oscillating energy of the free field into the definition of N_A, one gets:

$$\tilde{\mathcal{H}}_A^0 = \frac{p_A^2}{2} - \frac{1}{r_A} + \frac{l^2\omega^2}{4} + N_A\omega, \tag{22}$$

$$V_A^C = \frac{1}{r_A} - \frac{1}{|r_A + l\cos\phi|}, \tag{23}$$

$$0 \equiv \tilde{\mathcal{H}}_A^0 + V_A^C. \tag{24}$$

One sees at once that $\tilde{\mathcal{H}}_A^0$ is an integrable Hamiltonian, that generates the desired superposition of Coulomb motion (first two terms) and oscillatory

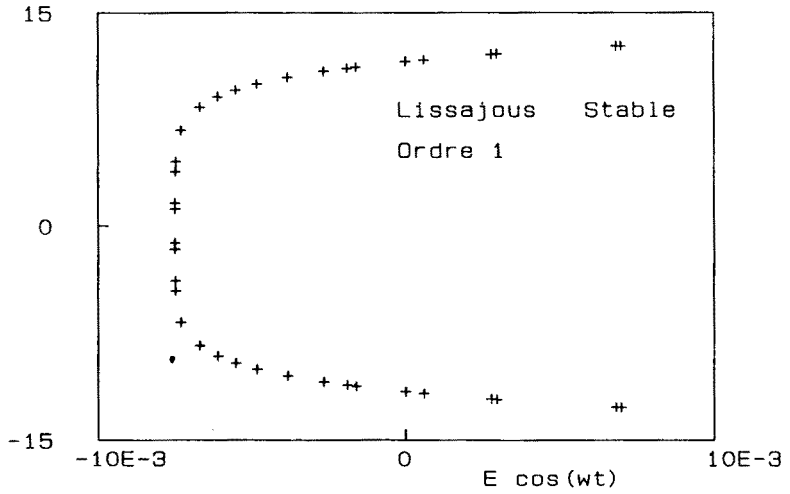

Fig. 10. Stable periodic orbit corresponding to the point S in Fig. 9. Shown is a Lissajous picture $\mu(t)$ as a function of $F\cos\omega t$. The driving field exerts a force $\vec{f} = -F\cos\omega t\vec{1}_\mu$, while the Coulomb force is always directed towards small μ. The number of points shown corresponds to the actual number of Richardson extrapolation steps.

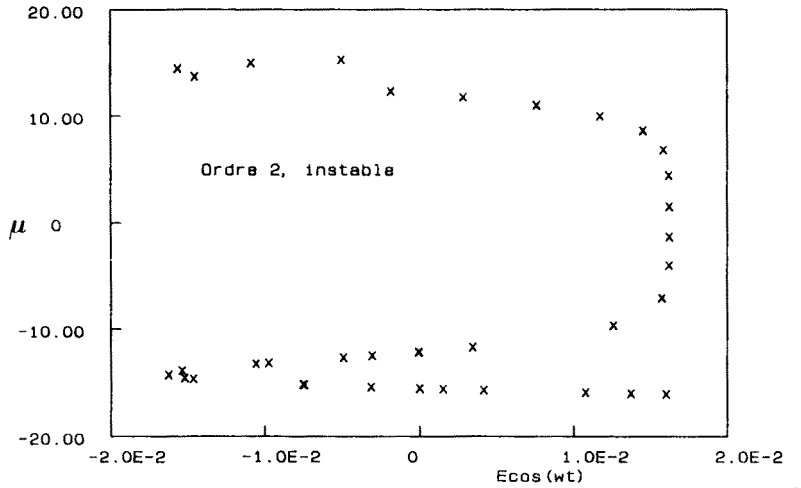

Fig. 11. Stable periodic orbit, period 2, corresponding to points U1,U2. Shown is a Lissajous picture $\mu(t)$ as a function of $F\cos\omega t$.

motion (signalled by the A-gauge). Also, the third term is the so-called ponderomotive potential term, which remains here at a constant value and sets the origin of the energy scale. The last term is just the energy of the free

electro-magnetic field. The coupling comes about through $V_{\rm A}^{C}$, mediated by the dynamical variables $r_{\rm A}$, ϕ.

Now, in a fashion parallel to Section 2.1., we switch to action-angle variables, taking due care whether the motion is instantaneously bound or unbound ($E \lesseqgtr 0$) [25,26]. If $I_{\rm A}$ is the usual Coulomb action, analogous to the quantum number n, but defined in the acceleration gauge, one has for the Coulomb part:

unbound motion	bound motion
$\mathcal{H} = \frac{+1}{2I_{\rm A}^2}$	$\mathcal{H} = \frac{-1}{2I_{\rm A}^2}$
$I_{\rm A} < 0$	$I_{\rm A} > 0$
$r_{\rm A} = 2I_{\rm A}^2 \sinh^2 u$	$r_{\rm A} = 2I_{\rm A}^2 \sin^2 u$
$p_{\rm A} = \frac{1}{I_{\rm A}} \coth u$	$p_{\rm A} = \frac{1}{I_{\rm a}} \cot u$
$\theta_{\rm A} = \sinh 2u - 2u$	$\theta_{\rm A} = 2u - \sin 2u$

(25)

$\theta_{\rm A}$ is the angle variable conjugated to $I_{\rm A}$ and u is the eccentric anomaly. The full free motion generator is now written as:

$$0 \equiv \tilde{\mathcal{H}}_{\rm A}^{0} = \mp \frac{1}{2I_{\rm A}^2} + \frac{1}{4} l^2 \omega^2 + N_{\rm A} \omega. \tag{26}$$

It is as simple and as complete as possible. If one likes to recast the Hamiltonian in its Lie group generators (see Section 2.1.), it would look like:

$$\tilde{\mathcal{H}}_{\rm A}^{0} = \frac{2}{\alpha} S_{3,A}^{(\alpha)} + \frac{1}{4} l^2 \omega^2 + N_{\rm A} \omega, \tag{27}$$

with $\alpha = \mp\sqrt{|2E|}$. The price to pay is that $V_{\rm A}^{C}$ cannot anymore be expressed in closed form, because of the Kepler law $\theta_{\rm A} = \theta(u)$ (Eq. (25)). However, its asymptotic limit is given by:

$$\lim_{r_{\rm A} \to \infty} V_{\rm A}^{C} = \lim_{\theta_{\rm A} \to \infty} V_{\rm A}^{C} = -l \cos\phi \frac{1}{I_{\rm A}^4 \theta_{\rm A}^2}, \tag{28}$$

recovering thus a rapidly decreasing perturbation.

Labelling of asymptotes is made on the basis of these action-angle variables $\{\theta_{\rm A}, I_{\rm A}; \varphi, N_{\rm A}\}$. As the angle variable has to remain finite, we define a reduced angle by analogy to [34]:

$$\psi_{\rm A}^{\rm As} = \varphi - \frac{\omega}{\Omega_{\rm A}^{\rm As}} \theta_{\rm A}^{\rm As}, \tag{29}$$

where the frequency $\Omega_{\mathrm{A}}^{\mathrm{As}} = \dot{\theta}_{\mathrm{A}}^{\mathrm{As}}$ is associated with the asymptotic Coulomb motion. Both $N_{\mathrm{A}}^{\mathrm{As}}$ and $\psi_{\mathrm{A}}^{\mathrm{As}}$ are finite and defined properly for any asymptotic time, independently of the phase of the stroboscopic Poincaré section.

3.5. Properties at infinity

3.5.1. Deflection functions

In order to stay consistent with our previous simulations we keep the same value of $F\omega^{-4/3} \simeq 0.1$, that determines the phase space structure. As is depicted in Fig. 9, that field is sufficently low so that the primary 1/1 elliptic resonance is still weakly connected to the asymptotic region; however the two elliptic secondary resonances remain and might influence the overall dynamics. Also, the previous studies of that system were performed at a definite frequency ω, in the CO_2 laser fequency range. We set thus $\omega = 0.004$ a.u. $\simeq 0.1$eV, thereby setting $F = 6.5$ a.u..

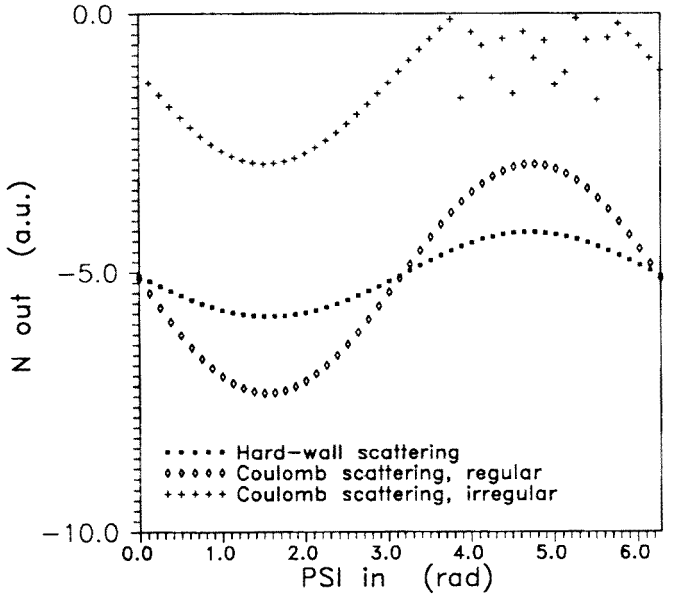

Fig. 12. *Overall regular, irregular Coulomb and hard-wall deflection functions.* Total deflection functions $N(\mathrm{out}) = N(\psi(\mathrm{in}))$ are shown for $0 \leq \psi(\mathrm{in}) < 2\pi$. For irregular scattering ($N(\mathrm{in}) = -1 \Rightarrow I_{\mathrm{A}} = 11.2$ a.u.), deflection function displays the coexistence of a regular region ($\psi < 3.8$ rad, $\psi > 5.7$ rad) and an irregular one, in between. Details are shown in Figs 13-14. At a higher incoming energy, ($N(\mathrm{in}) = -5 \Rightarrow I_{\mathrm{A}} = 11.2$ a.u.), only regular deflection is observed. Comparison is then made with scattering on a hard wall, with identical asymptotic energy.

Let us recall that we label the in-coming and out-going asymptotes by the asymptotic dynamical variables $N_{\mathrm{A}}^{\mathrm{As}}, \psi_{\mathrm{A}}^{\mathrm{As}}$, as defined in equation (29). A deflection function is just a mapping of in-coming into out-going asymptotes. In order to be able to derive inelastic cross-sections, we plot systematically $N_{\mathrm{A}}^{\mathrm{As}}(\mathrm{out}) = \mathcal{N}\left(\psi_{\mathrm{A}}^{\mathrm{As}}(\mathrm{in})\right)$, $0 \leq \psi_{\mathrm{A}}^{\mathrm{As}}(\mathrm{in}) < 2\pi$, for an arbitrarily chosen energy at infinity: $N_{\mathrm{A}}^{\mathrm{As}}(\mathrm{in}) = -1$. A full deflection function is depicted in Fig. 12, for $0 \leq \psi^{\mathrm{As}}(\mathrm{in}) < 2\pi$. The mechanism through which the irregular scattering shows up in the asymptotic regions is readily apparent. For $0\psi_{\mathrm{A}}^{\mathrm{As}} < 3.8$, the function is regular and displays a sine-like feature. It bears some similarity with scattering over a hard wall, with the same superimposed oscillating field. Accordingly, Fig. 12 also presents a typical defection function for hard-wall scattering with no multiple boucings. It shows the same general feature as the regular part of the Coulomb driven scattering; however, the amount of momentum exchange may be vastly different, as due to the singular character of $1/\left|r_{\mathrm{A}} - l\cos\phi\right|$ as $r_{\mathrm{A}} \to \infty$, and hence the impossibility to neglect non-linear couplings between field and particles in some region of space, for any set of parameters. This situation has been discussed in a different context by Casati *et al.* [22], in order to determine the outgoing electron energy, in a microwave ionisation experiment.

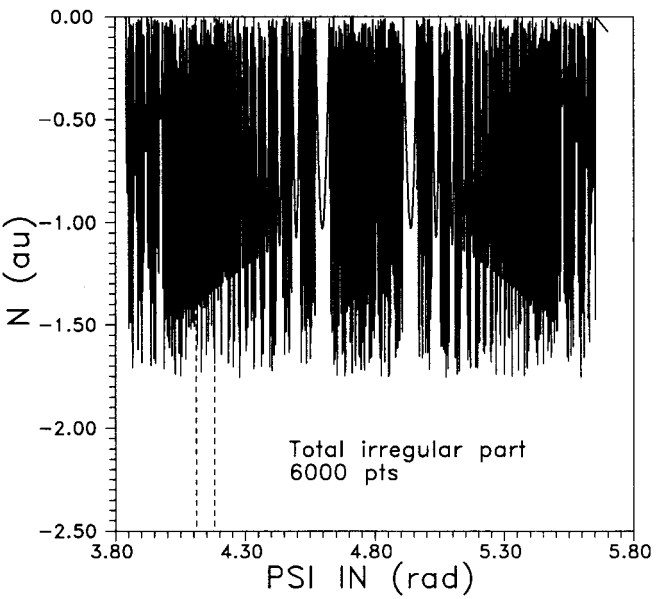

Fig. 13. Total irregular part of the deflection function $N(\mathrm{out}) = N\left(\psi(\mathrm{in})\right)$, with the same parameters as in Fig. 12. 6000 points simulation, the line connecting the points is a simple guide for the eye.

For $3.8 < \psi_A^{As}(\text{in}) < 5.7$, the deflection function is characteristic of a chaotic scattering process, as depicted in Fig. 13. The mechanism through which irregular scattering comes out in the deflection function is the following: as soon as the deflection curve would dive into bound states (resonances), with $N_A^{As}(\text{out}) \geq 0$, it is reflected back into the $N_A^{As}(\text{out}) > 0$ domainas the trajectory cycles one time more (or less) nearby a bound unstable periodic orbit. Its delay time, measured with reference to $\tilde{\mathcal{H}}_A^0$, jumps from $-\infty$ to $+\infty$ [15]. The different points on which such an accident occurs are the intersection of the periodic orbit stable manifolds with the plane at infinity. This explains how fractal-like structures appear in Fig. 13. A blow-up of the deflection function shows that the scattering behaviour in non-generic, at least for sufficiently a weak field. The fractal-like structure seems to have disappeared after a 10^3 magnification, (Fig. 14). While it is not clear yet whether the inner tori (tightly bound-states, elliptic islands) or the outer tori (Rydberg states) dominate the dynamics at long delays, the exponential scaling is clearly lost. Such a behaviour has been already described by Ott *et al.* [29], and is conjectured to be characteristic of a non hyperbolic chaotic saddle.

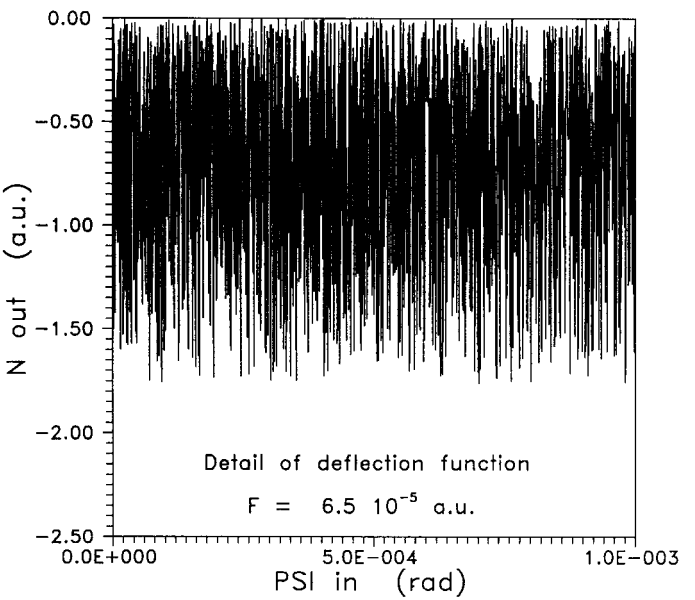

Fig. 14. Enlargement of Fig. 13, by a factor 225 (2000points/10^{-3}rad). The angle $\psi = \psi(\text{in}) - 4.13$. Any structure seems to have non-scaling behaviour of the scattering process.

3.5.2. Cross-sections

From the knowledge of deflection functions $N(\text{out}) = N(\psi(\text{in}))$, the classical differential cross-sections may be derived:

$$\left.\frac{d\sigma}{dN(\text{out})}\right|_{N=N_j} = \sum_{\psi_k} \left|\frac{dN(\text{out})}{d\psi(\text{in})}\right|^{-1}_{\psi(\text{in})=\psi_k}, \tag{30}$$

the sum being taken at the different ψ_k leading to N_j. A discontinuity (rainbow) in $d\sigma/dN$ occurs for each stationary point N_{st} in $N = N(\psi)$. One has $\lim_{N\to N_{\text{st}}-} d\sigma/dN = 0$ and $\lim_{N\to N_{\text{st}}+} d\sigma/dN = (N - N_{\text{st}})^{-1/2}$. The discontinuity is sharp and integrable, leading to a finite σ_{total}. Now, each generation of continuity g_i contributes to its own set of rainbows, but its integrated contribution will decrease with increasing generation i. For exponential scaling, the whole set of rainbows is a projection of the chaotic saddle fractal structure.

Of course, a deflection function like the one of Fig. 14 should contribute to nearly no integrated σ_{total}, even if the number of singularities is huge. This amounts to a practical limit to the number of peaks appearing in $d\sigma/dN$. The diffential cross-section $d\sigma/dN$ for the whole range of $\psi(\text{in})$ corresponding to irregular scattering is depicted in Fig. 15 and should show few more details at a more refined scale. Let us point out again that $d\sigma/dN$ is a way of labelling $d\sigma/dE$ (E, outgoing electron energy at infinity) by imposing equation (26) to hold in the asymptotic plane and by recalling $2I_{\text{A}}^{\text{As}} = E^{1/2}$.

It is most instructive to compare the cross-sections derived here with the quantum predictions of Kroll and Watson [32], which might at least give an order of magnitude of the exchanged energy. Let us recall that in the soft photon limit and with at most one resonance involved, one has for $N \lesssim 0$ photons:

$$\frac{d\sigma(N)}{d\Omega} = \frac{p(\text{out})}{p(\text{in})} J_N^2(\chi) \frac{d\sigma_0(\Delta p)}{d\Omega}. \tag{31}$$

$d\sigma_0(\Delta p)/d\Omega$ is the elastic cross section at $\Delta p = |\boldsymbol{p}(\text{out}) - \boldsymbol{p}(\text{in})|$, $\boldsymbol{p}$ being the electron momentum. $\chi = -A\alpha\Delta p/\omega(\text{a.u.})$ is the scaling parameter, as $J_N(\chi)$ decreases exponentially with N, if $N \gg \chi$. For our set of parameters, assuming $\Delta p \simeq (2E)^{1/2}$, $\chi = 0.36$. These lines ($N = N_{\text{elastic}} \pm \chi$) are shown in Fig. 15, together with the elastic line at $N_{\text{elastic}} = -1$. One sees that most of the $d\sigma/dN$ peaks fall well within the $N - N_{\text{elastic}} < \chi$ limit. It shows thus that even if the classical motion displays all characteristics of irregular scattering, the magnitude of the quantum of energy *in photon space* completely washes out any possible manifestation of chaotic behaviour in

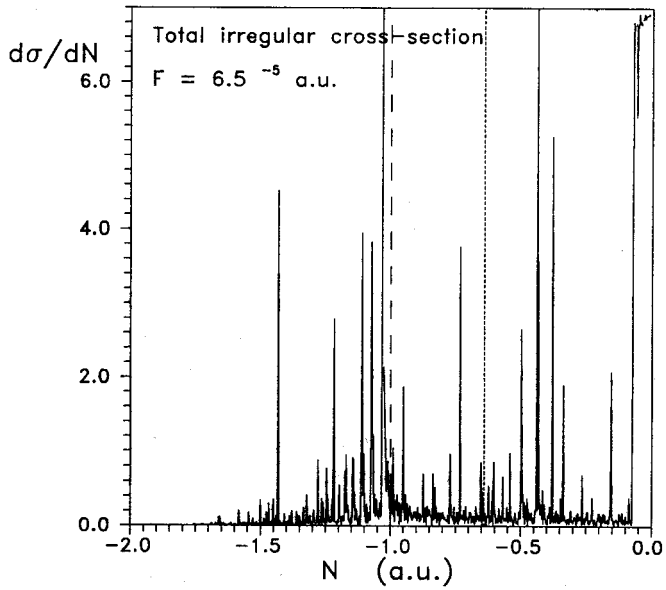

Fig. 15. Differential cross-section $d\sigma/dN$, with total σ normalized to unity. Deflection function of Fig. 13 is used for the derivation. Elastic scattering is shown as the dashed line, as well as the two lines $N_{\text{elastic}} \pm \chi$, as short-dashed lines (see text). The upsurge at $N > -0.05$ is due to numerical errors.

a semiclassical point of view. However, there seems to exist very few available quantum calculations in a Coulomb potential, even 1D, as underlined for example in reference [30]. A calculation was put forward [24], but in circular polarization of the field, which considerably simplifies the system. In Ref. [31] which also deals with circularly polarized light, the scaled parameters (with $\omega \simeq 0.37$ a.u.) are quite similar to ours. Unfortunately no $d\sigma/dE$ are presented. Let us thus consider the classical cross-sections as incentives for a quantum calculation, which could take into account the full symmetry of the Coulomb oscillator.

4. Conclusion

The Coulomb problem, perturbed by an external field, has two properties that make it lie at the heart of the microcopic chaos problem. First, and most important, it is readily accessible for the experimentalist, either through the observation of H and its excited states [28,27], or through the Rydberg states of the alkali atoms [12], or else by use of the external Coulomb potential of an ion. Second, the simplicity of the Hamiltonian, and the plain fact that it is perfectly known (in contrast to the vibrations

of nuclei or molecules) gives credit to the highly sophisticated experiments and calculations involved, and to the use of the powerful tools of group theory. It makes possible to shrink the non-integrable part of the dynamics to its smallest extent. However, the $1/r$ potential is known to be non-generic, with an essential singularity at infinity. One singularity at $r \to 0$ is easily removed, through regularization, and provides a coherent, simple picture of chaos at finite distances. If three particles interact with the $1/r_{ij}$ potential as in He^{**}, the situation would be more intricate as an essential singularity is created with all particles at a single point.

The situation at infinity is more diffcult to cope with, as that singularity is non-removable. If the perturbed motion is compared with ordinary free motion, infinite time delays and action integrals plague all calculations. It is a nessary perequisite to switch to a picture where the pure Coulomb motion is taken as the reference. That point of view is analogous of either the quantum defect approach to Rydberg states, or to the use of Coulomb–Born approximation in quantum scattering theory. However, the singularity at infinity being essential, the section at infinity is non-generic, as the Iterated Scattering map might show [16]. In the harmonically driven case, the coexistence of loosely and tightly bound trajectories complicates the analysis. The Fourier components of all the Coulomb states do not couple all at a time with the external driving frequency, leaving most untouched and the phase space of intrinsically mixed nature. An opportunity is thus given here to study chaotic scattering in a complex situation, and to look whether the global analysis put forward in the introduction do really apply here.

I gratefully thank the University of Kraków for its generous hospitality, as well as Dr A. Kleczkowski for his kind invitation. I also thank Prof. T. Tél as he kept on insisting on the special importance of a "complicated" case for classical chaotic diffusion.

REFERENCES

[1] R. Blümel, *Quantum Chaotic Scattering*, in *Directions in Chaos*, vol 4, Hao Bao Lin, ed., World Scientific, in press.
[2] W. Pauli, *Z. Phys.* **36**, 336 (1926).
[3] V. Bragmann, *Z. Phys.* **99**, 576 (1936).
[4] M. Bander, I. Itzykson,*Rev. Mod. Phys.* **38**, 330 (1966).
[5] A.O. Barut, R. Rącska, *Theory of Group Representations and Applications*, 2nd ed., World Scientific, Singapore 1982.
[6] D. Delande, Thèse d'Etat, Université Pierre et Marie Curie, Paris 1987.
[7] M.C. Gutzwiller, *Chaos in Classical and Quantum Mechanics*, Springer Verlag, New York 1990.

[8] H. Friedrich, D. Wintgen, *Phys. Rep.* **183**, 1 (1989).
[9] K. Richter, D. Wintgen, *Phys. Rev. Lett.* **65**, 1965 (1990).
[10] H. Hasegawa, M. Robnik, G. Wunner, *Prog. Theor. Phys. Supplement* **98**, 198 (1989).
[11] D. Delande, A. Bommier, J.C. Gay, *Phys. Rev. Lett.* **66**, 141 (1991).
[12] Chun-ho Iu, G.R. Welch, M.M. Kash, D. Kleppner, D. Delande, J.C. Gay, *Phys. Rev. Lett.* **66**, 145 (1991).
[13] L. Wiesenfeld, *Phys. Lett.* **A144**, 467 (1989).
[14] L. Wiesenfeld, *Comm. At.Mol.Phys.***25**, 335 (1991).
[15] L. Wiesenfeld, in *Proceedings of the Adriatico Research Conference on Quantum Chaos*, Trieste 1990, ed. by H. Cerdeira, World Scientific, Singapore 1991.
[16] L. Wiesenfeld, *J. Phys. B*, submitted for publication.
[17] T.A. Holme, R.D. Levine, *Chem.Phys.* **131**, 169 (1989); J. Hornos, F. Iachello, *J. Chem. Phys.* **90**, 5284 (1989).
[18] M.E. Kelmann, E.D. Lynch, *J. Chem. Phys.* **85**, 5855 (1986).
[19] U. Schramm, J. Berger, D. Habs, E. Jaeschke, G. Kilgus, D. Schwalm, A. Wolf, R. Neumann, R. Schuch, *Phys. Rev. Lett.* **67**, 22 (1991).
[20] F.B. Yousif, P. Van der Donk, Z. Zucherovsky, J. Reis, E. Brannen, J.B.A. Mitchell, T.J. Morgan, *Phys. Rev. Lett.* **67**, 26 (1991).
[21] R.V. Jensen, S.M. Susskind, M.M. Sanders, *Phys. Rep.* **201**, 1 (1991).
[22] G. Casati, I. Guarneri, D. Shepelyansky, *IEEE J. of Quant. Elec.***24**, 1420 (1988).
[23] J.G. Leopold, D. Richards, *J.Phys.B* **18**, 3369 (1985).
[24] L. Dimou, F.H.M. Faisal, *Phys. Rev. Lett.* **59**, 872 (1987).
[25] R. Graham, *Europhys.Lett.* **7**, 671 (1988); R. Graham, M. Höhnerbach, *Phys. Rev. Lett.* **64**, 637 (1990).
[26] C. Jung, *Scattering chaos in the harmonically driven Morse system*, private communication, 1991.
[27] R. Blümel, A. Buchleitner, R. Graham, L. Sirko, U. Smilansky, H. Walther, *Phys. Rev.* **A44**, 4521 (1991).
[28] D. Richards, J.G. Leopold, P.M. Koch, E.J. Galvez, K.A.H. van Leeuwen, L. Moorman, B.E. Sauer, R.V. Jensen, *J.Phys.B* **22**, 1307 (1989).
[29] Y.T. Lau, J.M. Finn, E. Ott, *Phys. Rev. Lett.* **66**, 978 (1991).
[30] M. Pont, R. Shakeshaft, *Phys. Rev.* **A43**, 3764 (1991).
[31] A. Franz, H. Klar, J.T. Broad, J.S. Briggs,*J.Opt. Soc. Am.* **B7**, 545 (1990).
[32] N.M. Kroll, K.M. Watson, *Phys. Rev.* **A8**, 804 (1973).
[33] C. Cohen-Tannoudji, J. Dupont-Roc, G. Grynberg, *Photons et Atomes: Introduction à l'Electrodynamique Quantique*, InterEditions, Paris 1988.
[34] U. Smilanski, in *Chaos and Quantum Physics*, M.-J. Giannoni, A. Voros, Zinn-Justin, eds, Les Houches session LII, Elsevier 1991 (in the press).